






Generation and annihilation of skyrmions and antiskyrmions in magnetic heterostructuresSabri Koraltan ^{1,2,*}, Claas Abert ^{1,3}, Florian Bruckner ¹, Michael Heigl ⁴, Manfred Albrecht ⁴, and Dieter Suess^{1,3}¹*Faculty of Physics, University of Vienna, Kolingasse 14-16, A-1090, Vienna, Austria*²*Vienna Doctoral School in Physics, University of Vienna, Kolingasse 14-16, A-1090, Vienna, Austria*³*Research Platform MMM Mathematics - Magnetism - Materials, University of Vienna, Vienna 1090, Austria*⁴*Institute of Physics, University of Augsburg, Augsburg 86159, Germany*

(Received 10 August 2022; accepted 15 September 2023; published 2 October 2023)

We demonstrate the controlled generation and annihilation of (anti)skyrmions with tunable chirality in magnetic heterostructures by means of micromagnetic simulations. By making use of magnetic (anti)vortices in a patterned ferromagnetic layer, we stabilize (anti)skyrmions in an underlying skyrmionic thin film in a reproducible manner. The stability of the (anti)skyrmion depends on the polarization of the (anti)vortex, whereas their chirality is given by those of the (anti)vortices. We investigate the influence of geometric parameters such as nanodisk radius and film thickness on the stability of the (anti)skyrmions. By introducing the interlayer Dzyaloshinskii-Moriya interaction into our modeling, we predict that the same coupling mechanism works also for chiral skyrmions. Furthermore, we demonstrate that the core coupling between the (anti)vortices and (anti)skyrmions allows deleting and writing of spin objects in a controlled fashion by applying short pulses of in-plane external magnetic fields or charge currents, representing a new key paradigm in skyrmionic devices.

DOI: [10.1103/PhysRevB.108.134401](https://doi.org/10.1103/PhysRevB.108.134401)**I. INTRODUCTION**

Magnetic textures with nontrivial magnetization states have been intensively researched since the first discovery of skyrmions [1–4]. The skyrmions are local whirls in the out-of-plane magnetization. The most common way to stabilize skyrmions is to use a magnetic material where the inversion symmetry is broken due to the Dzyaloshinskii-Moriya interaction (DMI) [5–7]. Another typical stabilization mechanism is to make use of the competing interaction between long-range dipolar interactions and short-range exchange interactions in a magnet with perpendicular magnetic anisotropy (PMA) [8–10].

Magnetic skyrmions are topologically protected in the sense that their magnetization configuration cannot be transformed into the ferromagnetic state by a continuous uniform transformation [11]. This protection makes them robust against external stimuli, such as magnetic fields. Thus, multiple devices have been proposed in which one can make use of the increased stability, such as racetrack memory, reservoir computing, or skyrmion oscillators [6,12–17]. In the concept of the skyrmion race track, the information is encoded in the distance between skyrmions [18]. However, the nonconstant velocities of individual skyrmions, the skyrmion Hall effect, and the pinning sites on the racetracks have shown that this principle of storage is challenging in its current stage [19,20].

An alternative storage principle has been proposed with the discovery of antiskyrmions [21,22]. Namely, the skyrmion could store the bit 0, whereas the antiskyrmion could store the bit 1 [23]. So far, only a handful of materials have been known to host both skyrmions and antiskyrmions. Several Heussler compounds can host skyrmions and antiskyrmion lattices under different conditions [24–26], therefore, not simultaneously. The second class of material that can cohost both skyrmions and antiskyrmions are ferrimagnetic Fe/Gd-based multilayers [10]. Here, the spin objects are nucleated by shrinking of the chiral domain walls as well as the wall junctions in an applied field. Regardless, the random distribution of the spin objects and the lack of controllability of their nucleation and annihilation raise new challenges for the development of skyrmion-antiskyrmion racetrack devices.

In this work, we present a micromagnetic study in which we model a ferrimagnetic layer with low saturation magnetization and low PMA, in which we can control coexisting skyrmions and antiskyrmions. On top of this skyrmion hosting layer (SkL), we put a nanodisk array or a square lattice made out of a soft magnetic material such as permalloy. In these structures, vortices or antivortices can be nucleated, as illustrated in Figs. 1(a) and 1(b), respectively. Based on the (anti)vortex core polarity in the upper vortex layer (VL), we can nucleate skyrmions and antiskyrmions. We investigate the tunability of the proposed stabilization mechanism by varying the nanodisk radius and film thickness, and probe the influence of interfacial DMI strength on the stability of the spin objects. Furthermore, we demonstrate that the spin objects in SkL can be annihilated if the polarization of the (anti)vortices core in the vortex layer (VL) is reversed by a short pulse of an in-plane magnetic field. Local pulses of current are also investigated to test the feasibility of the deleting operation. Controlled nucleation and annihilation of

*Corresponding author: sabri.koraltan@univie.ac.at

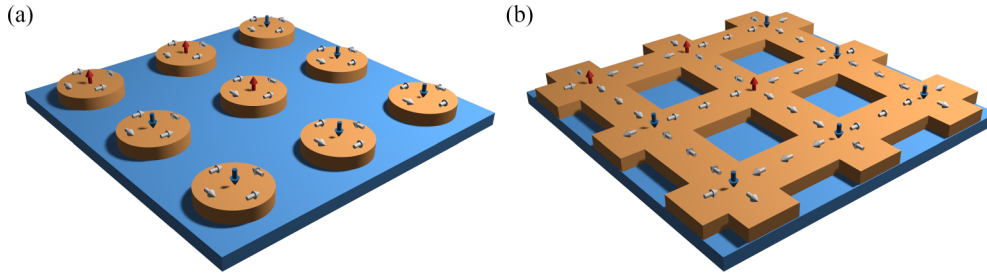


FIG. 1. Schematic illustration of the proposed heterostructures, (a) a vortex layer (VL, orange) is situated on top of a skyrmion host layer (SkL, blue). The arrows show the magnetization in the VL. In (a), we schematically show magnetic nanodisks. The radius R of the nanodisks with thickness t_{VL} can be varied to arrange the skyrmions in the SkL with the desired periodicity. A further tuning parameter is the lattice constant a that describes the disk center to disk center distance. In (b), we illustrate that the square lattice can be used as the VL, where following studies on frustrated spin systems, stable antivortices can be obtained by means of alternative field demagnetization protocols.

the (anti)skyrmions in arbitrary patterns represent a significant step toward skyrmion-based memory and computing devices.

This paper is organized as follows. Details of the micromagnetic simulations are provided in Sec. II, followed by the structural modeling of the proposed heterostructures. The main findings are presented and discussed in Sec. III, where we give a deeper insight into the relaxation mechanisms of the spin textures and the deletion process of (anti)skyrmions. We support the main findings with our Supplemental Material, discussing the variation of geometrical parameters, the influence of DMI, and energy barrier calculations for the stability of coupled skyrmion-vortex pairs. We summarize and conclude our results in Sec. IV.

II. MODELING

A. Micromagnetic modeling

We will start this section by choosing appropriate material parameters for the SkL and VL, as these will not change for the rest of the manuscript. The SkL is modeled as a ferromagnet with low saturation magnetization $M_s^{\text{SkL}} = 225 \text{ kA/m}$, low PMA $K_u^{\text{SkL}} = 22.4 \text{ kJ/m}^3$, and an exchange stiffness constant $A_{ex}^{\text{SkL}} = 6 \text{ pJ/m}$. The material parameters are chosen according to a previous work [10]. For the VL, we choose material parameters similar to permalloy (NiFe) with $M_s^{\text{VL}} = 800 \text{ kA/m}$, $K_u^{\text{VL}} = 0 \text{ kJ/m}^3$, and $A_{ex}^{\text{VL}} = 13 \text{ pJ/m}$ [27].

For our micromagnetic investigations, we use `magnum.np`, a finite-difference-based micromagnetic simulation framework [28]. To do so, we discretize the magnetic system into cuboids of constant volume $V = (l_x \times l_y \times l_z) = (5 \times 5 \times 10) \text{ nm}^3$. The number of cells used for each system may vary, so we indicate this separately while discussing the results. However, except for thickness dependence investigations, we keep the number of cells along the z -axis constant, $n_z = 8$, where the first five are used as SkL, and the last three for VL.

In `magnum.np`, we include energy contributions from demagnetization, anisotropy, exchange, and external fields into the effective field term of the magnetic system [29]. We then solve the Landau-Lifshitz-Gilbert equation considering this effective field. As we are primarily interested in equilibrium states, we perform numerical investigations with a high Gilbert damping parameter, where $\alpha = 1$. For the

deleting and writing simulations, we decrease this value to $\alpha = 0.1$.

Note that the skyrmions and antiskyrmions have an opposite winding number

$$N(\mathbf{m}(t)) = \frac{1}{4\pi} \mathbf{m}(t) \cdot \left(\frac{\partial \mathbf{m}(t)}{\partial x} \times \frac{\partial \mathbf{m}(t)}{\partial y} \right) dx dy, \quad (1)$$

where $\mathbf{m}(t)$ is the time dependent normalized magnetization vector. While the winding number, or the skyrmion number, is supposed to be an integer number, an invariant representing the topology of the spin object, with our micromagnetic code we can calculate N at each time step t . Thus, this will allow us to quantify any changes in the topology, e.g., nucleation or annihilation of (anti)skyrmions.

B. Nanodisk array - Magnetic vortices

The first geometry we investigate is obtained by patterning the permalloy layer into a 2D nanodisk array. Fabrication of such structures could be achieved by electron or photolithography (depending on the sizes of the nanodisk) and a typical lift-off technique [30]. Similar structures have been experimentally realized investigating 2D spin systems [31]. Note that depending on the ratio between the thickness and radius of the nanodisks, magnetic vortices are stable magnetic configurations, which are crucial for the nucleation of skyrmions in SkL [32].

Figure 1(a) illustrates a square nanodisk lattice that is being prepared on top of the SkL. Several parameters can be tuned within the lattice, such as the radius of the nanodisks R , the thickness of the nanodisks t_{VL} , as well as the lattice parameter a that defines the center-to-center spacing between two disks. If not stated otherwise, the parameters used for the nanodisk array are $R = 200 \text{ nm}$, $t_{VL} = 30 \text{ nm}$, and $a = 500 \text{ nm}$.

By coding the angle of the magnetization with the color wheel shown in Fig. 2, we can illustrate all three components of the magnetization of a magnetic vortex with its in-plane magnetization rotation [Fig. 2(a)] and its core highlighted by the m_z component as shown in Fig. 2(b).

C. Square lattice - Magnetic antivortices

Even though a nanodisk could be used to stabilize an antivortex, we find it more feasible to switch the geometry of the

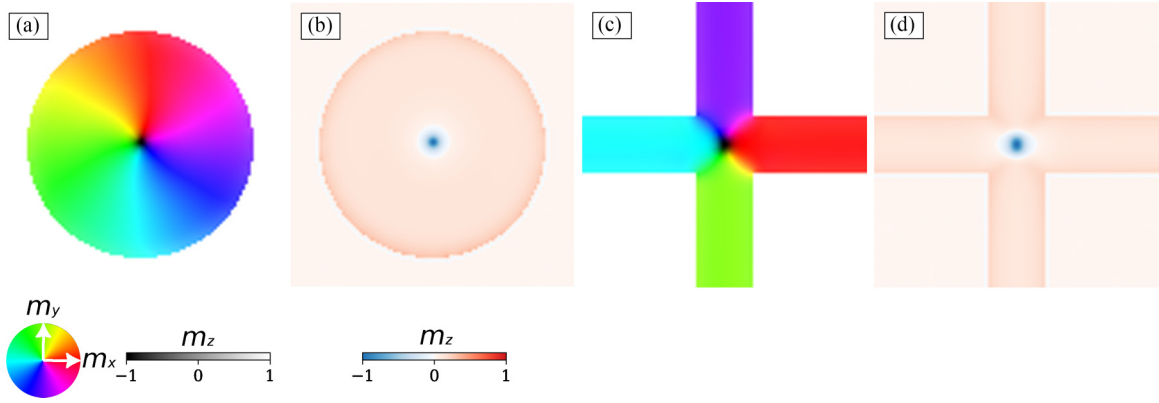


FIG. 2. Representative illustration of a magnetic vortex. In (a) we illustrate the IP rotation of the magnetic vortex core via the color-coded color wheel, and in (b) we show the m_z component of the vortex, where the vortex core has a negative polarity. The magnetization configuration of an antivortex stabilized in the VL is depicted in (c) and (d).

VL into a well-studied system where antivortices are known to be present: The interconnected square lattice. Such lattices have been intensively investigated within the field of artificial spin ices (ASI) [33,34].

In these square lattices there is a long-range ordered magnetic ground state [35]. Here, the magnetization in each vertex follows an antiferromagnetic arrangement, where opposing elements have an antiparallel magnetization. Two elements are oriented to the center, while the other two are oriented away from the center. Thus, an antivortex rises at the center of the vertex, at the junction of the elements. Hence, we used this magnetic configuration to stabilize antivortices in the VL. Note that such states can be experimentally realized by applying a demagnetizing protocol, where the external magnetic field rotates in the plane of the lattice and has an amplitude that decreases with time [33].

Taking into account the illustration from Fig. 1(b), the square lattice can be described by the width of the lattice element w instead of the radius R of the nanodisk lattice. The other parameters t_{VL} and a are still valid here. If not specified otherwise, we use $w = 100$ nm.

An antivortex which is stabilized in the square lattice is shown in Figs. 2(c) and 2(d). In the following sections, we discuss the vortex-skyrmion and antivortex-antiskyrmion coupling in more detail.

III. RESULTS

A. Vortex core-skyrmion coupling

We start our micromagnetic computation with an initial magnetization state, where the nanodisks in the VL all have stable vortices (clockwise chirality), whereas the SkL has a cellwise random magnetization configuration. We relax the magnetization with respect to its total energy by solving the LLG numerically. We simulate the response of our system to an OOP magnetic field that increases 2 mT every 10 ns. The obtained M-H hysteresis loop is shown in Fig. 3(a). Supported by the magnetization states given in the red and blue panels, we can see that no skyrmions are found in the SkL at zero field. However, we can recognize ringlike magnetic domains concentrated at the nanodisk locations. Simultaneously, all nanodisks have one magnetic vortex of equal polarity and

chirality. Increasing the OOP field, the stripelike domains are shrinking into Bloch skyrmions. We observe that the skyrmion and vortex cores are coupled to each other in the sense that the vortex imprints its chirality and polarity on the SkL, where the PMA leads to the formation of a skyrmion. Without loss of generality, we can say that a skyrmion is nucleated beneath a vortex core, if the applied external magnetic field is antiparallel to the polarity of the vortex core. However, this does not always happen in the initial field protocol if we start from the randomly magnetized skyrmion layer. Nevertheless, we can stabilize skyrmions at each nanodisk location by saturating the SkL, reversing the magnetic vortex core by the applied OOP field, and decreasing the magnetic field back to negative values. Note that the vortex core radius is essential for the stability of the skyrmion underneath.

To better understand under which conditions the skyrmions and vortices are stable, we provide energy barrier calculations using the string method [29,36] in the Supplemental Material [37]. The magnetization state with the least energy is the one in which the vortex core is parallel to the applied field and the SkL is saturated. If the vortex core is reversed, the exchange energy increases as the vortex core and the SkL are now in opposition. If there is a skyrmion in the SkL, the total energy of the system will be even higher, since one skyrmion is more energetically costly than the saturated state of the SkL. These three states are energetically allowed. The state with a skyrmion, but with the vortex core pointing in the same direction as the applied OOP field and in opposition to the skyrmion core, is not stable.

The energy barrier between the vortex-skyrmion coupled state and the magnetization state without a skyrmion exists despite the fact that the vortex core has the appropriate polarity. Our understanding of the skyrmion stabilization mechanism from the M-H hysteresis loops reveals that skyrmions can be stabilized beneath a magnetic vortex core with a polarity opposite to the applied out-of-plane field, provided the domain morphology of the skyrmion lattice at remanence allows its formation through the shrinking of a domain. If the domain beneath the vortex core is parallel to the applied field and already in a nearly saturated state, then a skyrmion cannot be stabilized. Therefore, it is necessary to saturate the SkL and return to remanence, and then switch the polarity of the

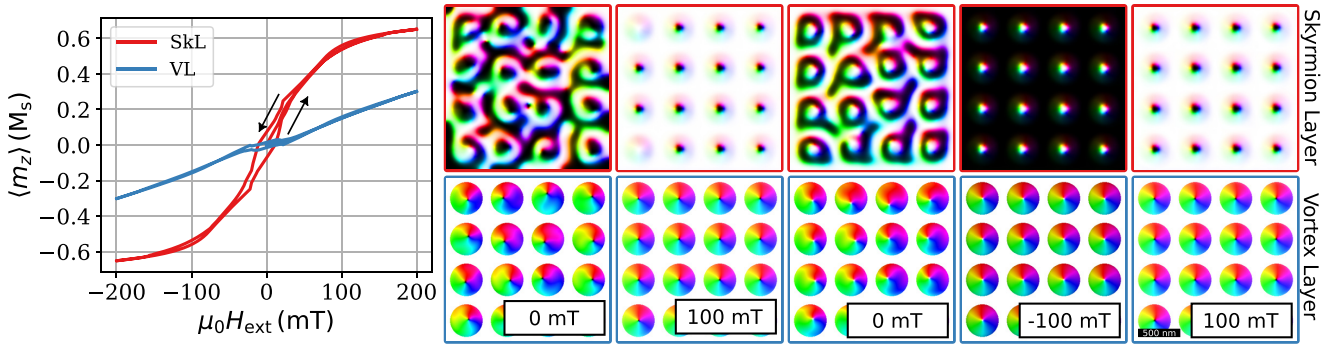


FIG. 3. Simulated out-of-plane M-H hysteresis loop where the m_z component of the magnetization is averaged over the SkL (red) or VL (blue). Magnetization configurations along the hysteresis loop are illustrated in the corresponding color panels at chosen magnetic fields. Scalebar corresponds to 500 nm.

OOP field to obtain the full lattice of skyrmions. Note that the energy barriers calculated using micromagnetic theory are quantitatively inaccurate if Bloch points are involved in the nucleation (annihilation) process. Thus, we focus solely on a qualitative analysis here. This formation mechanism is highlighted in the cross section of the magnetization at chosen OOP fields from Fig. 4.

The proposed and numerically demonstrated skyrmion nucleation mechanism has the advantage that one can tune the geometry of the VL and alter the properties of the skyrmions in the SkL. In the Supplemental Material [37], we investigate in more detail how the radius of the nanodisk allows us to tune the density of the skyrmions. Similarly, the lattice constant will lead to the same result. Furthermore, due to the strong exchange coupling between SkL and VL, a critical thickness of the SkL exists for which the skyrmions are not in-plane imprints, but rather form Bloch skyrmions with OOP surrounding magnetization. The critical thickness is at $t = 40$ nm.

As chiral skyrmions are intensively investigated for skyrmion-based devices, we now add interfacial DMI into our system that is assumed to originate from a heavy-metal layer positioned underneath the SkL. The results are summarized in the Supplemental Material [37]. The stability and chirality of the skyrmions are not significantly influenced by the additional DMI in the system. If a certain threshold is exceeded, then spin spiral states are obtained. Overall, we can conclude

that the proposed method works for both dipolar and chiral skyrmions.

B. Antiskyrmions and Antivortices

Within our study, the role of the vortex core is to nucleate the skyrmion core, but the disk IP magnetization configuration gives the skyrmions IP texture and chirality. Thus, we are now using the square lattice as the VL in which the long-range ordered ground state contains antivortices at the vertex centers. This ground state can be obtained by either thermal activation or demagnetization protocols. The former works well for very thin systems [38,39] and the latter for thicker elements [33,34].

As in the case of the nanodisk array, we initialize the VL in the desired state, and then simulate the system's response to an OOP magnetic field. Figure 5 depicts the obtained M-H hysteresis loop with the corresponding magnetization states at relevant magnetic fields. In the central region, where each vertex has four full-sized elements, an antiskyrmion can be stabilized after ramping the field up and down.

Figure 6 reveals a strong exchange coupling between the antivortex and antiskyrmion. The stabilization mechanism discussed above for the nanodisk is still valid: If the vortex core polarity is opposed to the direction of the applied field, an antiskyrmion can nucleate. For completeness, we investigate the role of element width and film thickness in antiskyrmion

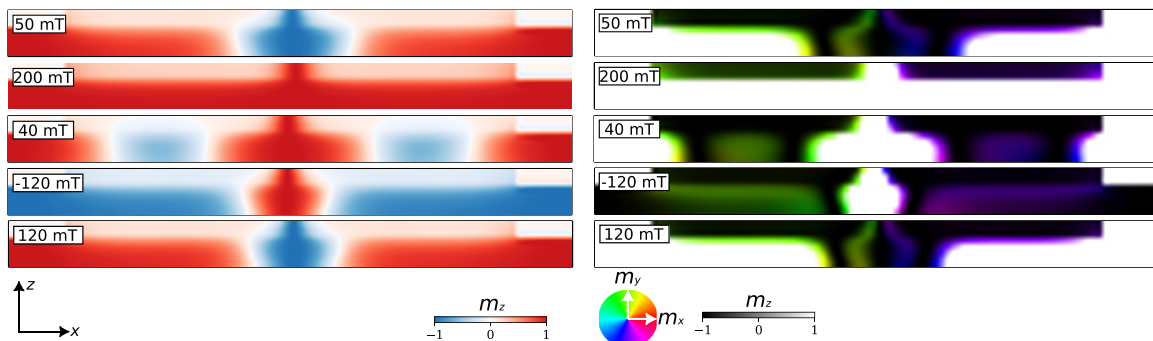


FIG. 4. Cross-sectional view of a coupled vortex and skyrmion in the xz plane at different OOP fields obtained from the hysteresis simulation shown in Fig. 3. The left panel shows only the z component of the magnetization, while the right panel uses the color-coded representation. The 3D coupled skyrmion-vortex texture can be stabilized with both polarities based on the direction of the applied magnetic field.

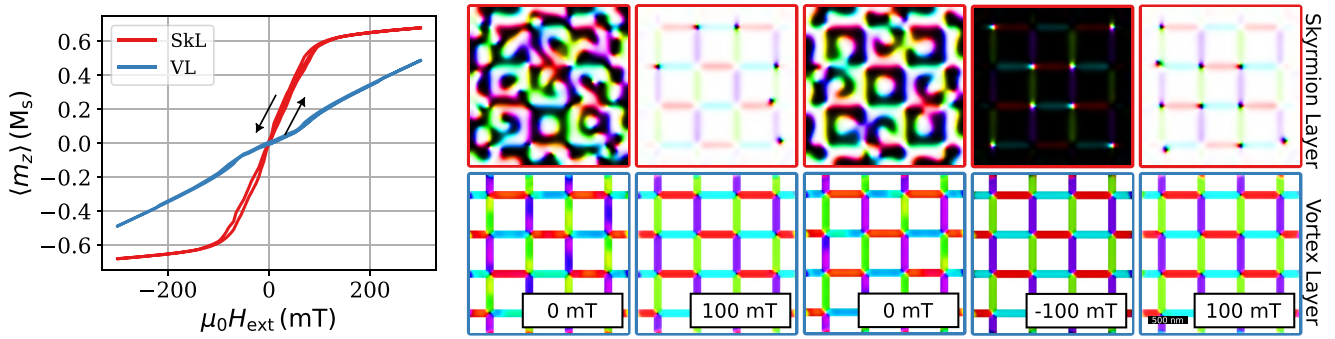


FIG. 5. The same as Fig. 3 if a square permalloy lattice is the VL, and the initial magnetization state contains only the antivortex and antiferromagnetic arrangement of the lattice sites in the VL, as shown in the blue panel on the right with the color-coded magnetization configurations. Antiskyrmions are stable at the different magnetic fields in the SkL, as illustrated in the red panel.

stabilization; see the Supplemental Material [37] for more details. The width of the element does not significantly impact the stability of antiskyrmions. The film thickness is critical for the proposed concept to work, as too thin films will result in rather IP magnetized states. Furthermore, we find that there exists an allowed DMI threshold for which the antiskyrmions remain stable skyrmion solutions in our system.

C. Field pulse driven skyrmion and antiskyrmion annihilation

One of the main challenges to realize a skyrmion-based memory device is the controlled annihilation of the spin objects. Especially in a two-object approach, where skyrmions and antiskyrmions encode bits “0” and “1”, respectively, it is important to delete and write the information as desired. With our approach, we have so far shown that we can nucleate the spin textures at the desired location. We will now focus on how to annihilate them. For simplicity and to reduce simulation time, we will consider only one pair of (anti)vortex (anti)skyrmion where the width of the square lattice element is reduced to $w = 50$ nm.

As we have seen in the previous sections, the polarity of the magnetic vortex (antivortex) core determines the existence of a skyrmion underneath. We aim to switch the polarity of the vortex core and ultimately delete the skyrmion underneath.

Similarly to well-studied magnetic vortex core reversals [40–43], we apply an IP magnetic field pulse with a full width at a half maximum of $\sigma_{\text{pulse}} = 100$ ps. To better understand the

limits of the switching process, we vary both the applied OOP bias field to stabilize the skyrmions H_{bias} and the magnitude of the applied IP pulse H_{pulse} .

D. Annihilation of Skyrmions

Figures 7(a) and 7(b) show the computed winding number after the field pulse was applied and the system was relaxed for an additional nanosecond. We see a clear correlation between the vortex core reversal success ($N < 0$ switched to $N > 0$) from Fig. 7(a) and the topological number at the end of the simulation in the SkL, where $N = -1$ indicates that the skyrmion is still there, while $N = 0$ reveals that the skyrmion was deleted. Figures 7(c) and (d) show the temporal evolution of N for the vortex (c) and the skyrmion (d) for different pulse magnitudes in a constant OOP field of 100 mT. We observe that there exists a clear critical pulse magnitude based on the chosen bias field. The transition appears rather smoothly, even though the annihilation mechanism is quite complex, as illustrated in Fig. 8. Vortex core annihilation starts by creating a vortex-antivortex core pair. The vortex core reversal is completed once the original vortex core vanishes. Underneath, the process is more complex. By destroying the coupling between the skyrmion and the vortex core, the skyrmion’s topological protection is broken and follows a rather complex transformation to a trivial-bubble-like structure in the nonequilibrium state, which then vanishes quickly.

Ultrafast field- or current-induced magnetic vortex core reversal is a repeatable process [27]. Thus, one would expect

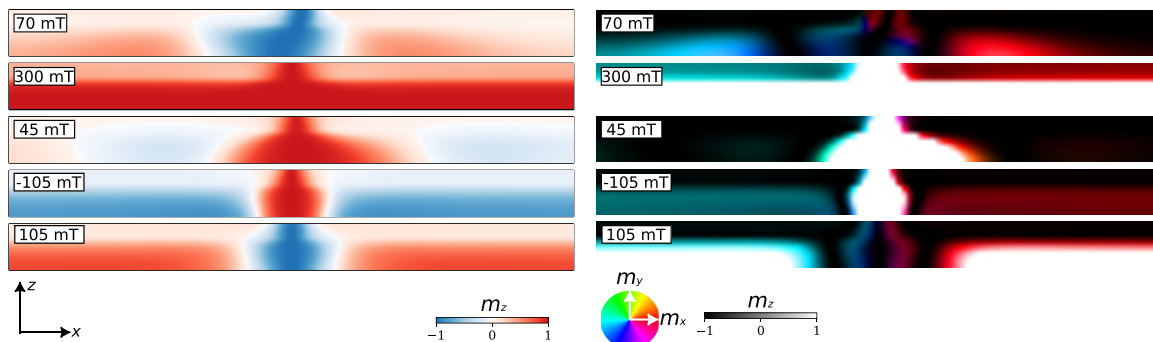


FIG. 6. The same as Fig. 4 but for an antiskyrmion that is coupled to the antivortex from the VL.

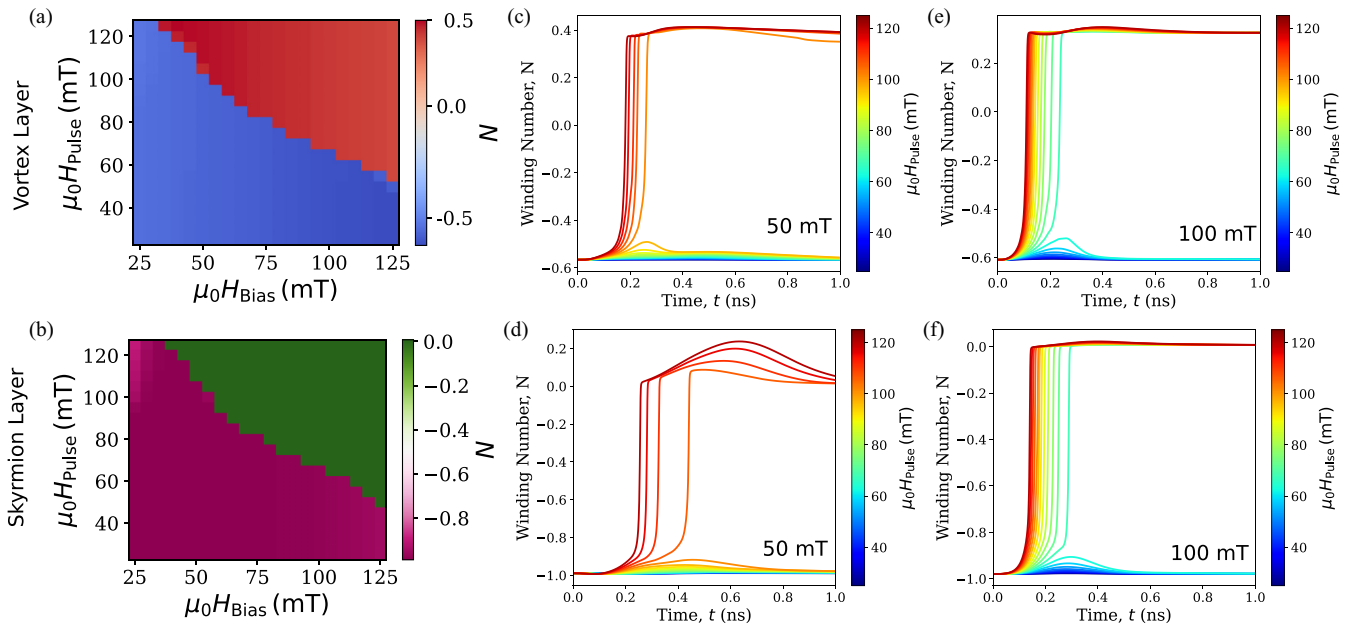


FIG. 7. Phase diagrams describing the topological state of the single vortex-skyrmion structure after being subject to an IP magnetic field pulse of Gaussian shape, wherein (a) the topological number of the VL is shown as a function of the chosen constant OOP bias field H_{bias} , and the amplitude of the IP magnetic field pulse H_{pulse} , and in (b) the topological number of the SkL, where for values around $N = 0$ the skyrmion is deleted via the vortex-core reversal. The temporal evolution of N for different magnitudes of the IP field pulse is shown in (c)–(f), where the amplitude of the bias field is written inside the figures.

that one could write a skyrmion by applying an IP pulse of magnetic field to a ferromagnetic state. In the Supplemental Material [37], we demonstrate that this is true in some cases but also quite difficult to achieve reliably. One needs to reduce the OOP bias field to be able to write a skyrmion. In a realistic, large magnetic system, this might lead to undesired new spin objects.

Another critical aspect of the writing/deleting mechanisms is that reversing a vortex core can be realized using charge

or spin currents to ensure a local operation. We investigate the switching behavior by applying a short pulse of an IP current; see the Supplemental Material [37] for more details. The spin transfer torque (STT) acts on the local gradient of the magnetization, in this case the vortex core, and results in the formation of vortex-antivortex pairs, which ultimately annihilate the original vortex [27]. This approach addresses the issue of locality since it is possible to design the vortices in such a way that the current is applied only locally

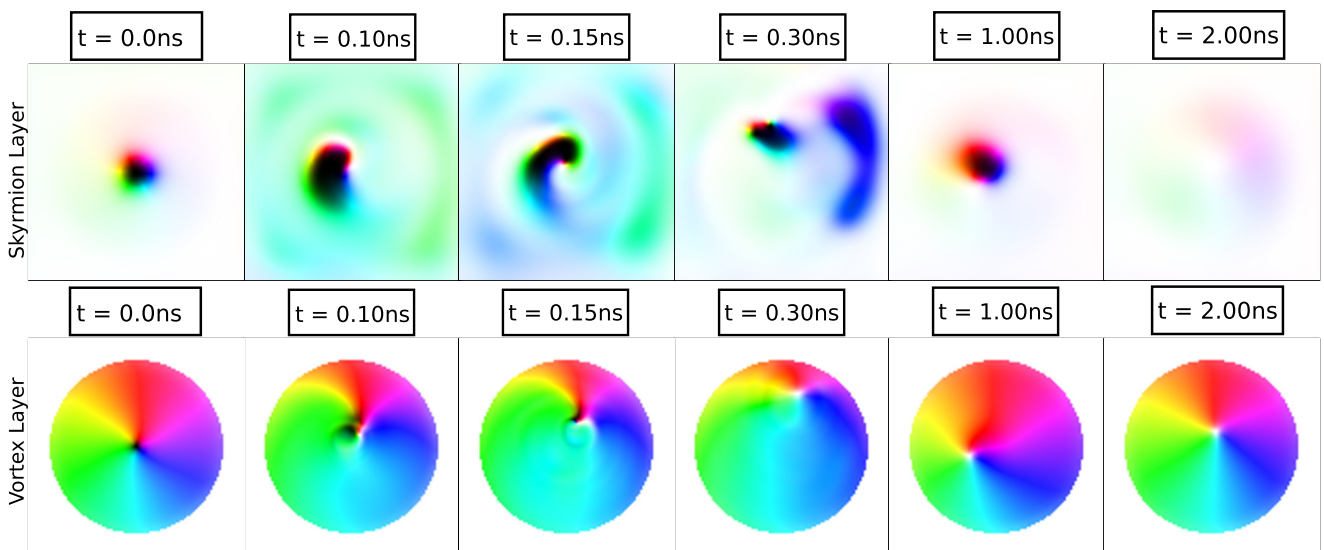


FIG. 8. Evolution of the magnetization configuration during the vortex core reversal process induced by a short IP magnetic field pulse. The upper panel illustrates the skyrmion vanishing after $t = 2$ ns, and the lower panel depicts how the vortex core reverses its polarity [-1 (black) to $+1$ (white)] by nucleating an additional antivortex and subsequent vortex-antivortex-pair annihilation.

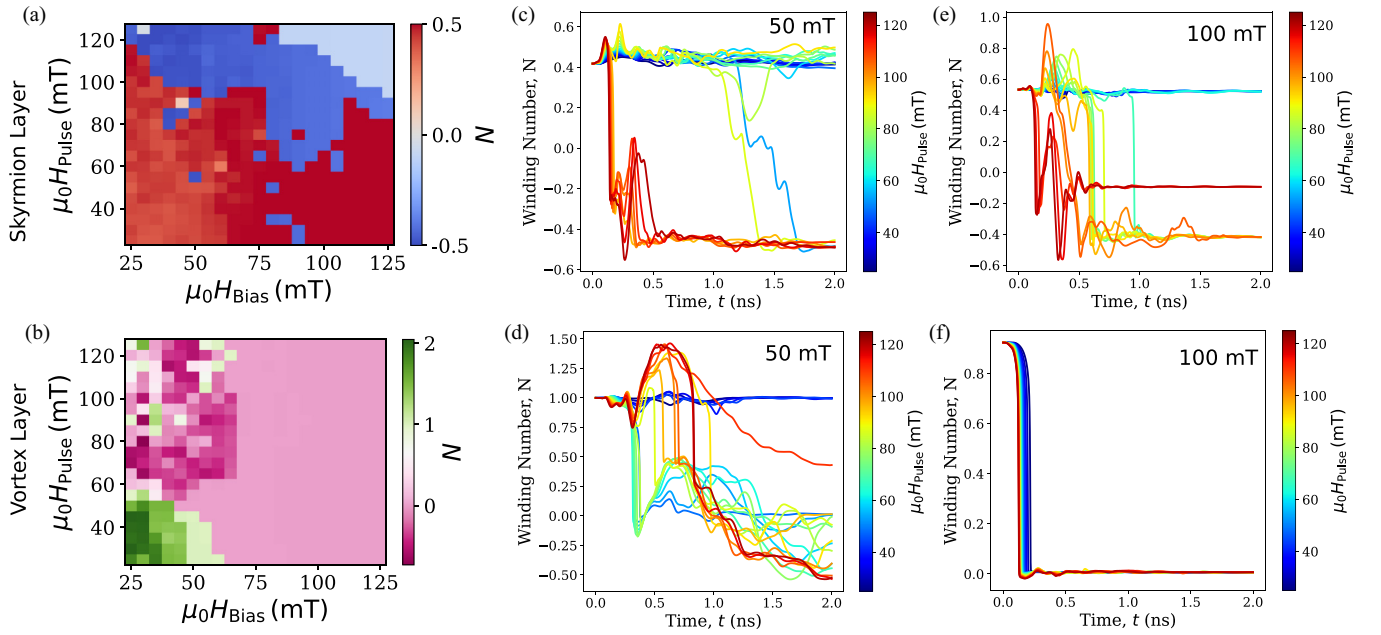


FIG. 9. Same as Fig. 5 but for an antiskyrmion in the SkL and an antivortex in the VL using a square lattice.

in an experimental setup. Although the required IP current amplitudes are very high, the pulses have a standard deviation of less than 1 ns. Therefore, it should be feasible to achieve the high current densities without causing strong Joule heating.

E. Annihilation of Antiskyrmions

In the same manner, we demonstrate the first controlled antiskyrmion annihilation with a pulse of the external magnetic field, as illustrated in Fig. 9. The OOP field is set to $\mu_0 H_{bias} = 100$ mT. The pulse has a maximal value of $\mu_0 H_{pulse} = 70$ mT with a duration $\sigma = 80$ ps. In contrast to the vortex-core reversal, the antivortex core seems to depend strongly on the lattice geometry. Additionally, the correlation between antivortex core reversal shown in Fig. 9(a) and antiskyrmion annihilation from Fig. 9(b) is not as clear as in the skyrmion case. While the two phase diagrams show no real correlation, the temporal evolution of N shown in Figs. 9(c) and 9(d) also suggests that the annihilation process may be independent of the antivortex core reversal. Nevertheless, we see that the idea works again in principle, as we can understand from the magnetization states during the annihilation process depicted in Fig. 10. However, the conditions to make this mechanism more deterministic and reliable must be investigated in more detail.

IV. CONCLUSIONS AND DISCUSSION

In this paper, we use micromagnetic simulation to describe the vortex-skyrmion coupling in magnetic heterostructures consisting of a vortex nanodisk array and a skyrmionic layer that can host skyrmions independently. We showed that a 2D array of nanodisks could be utilized to control the nucleation of skyrmions in a lattice where an OOP field is applied. The vortex core assists the nucleation of the skyrmions, whereas

the antiskyrmions can be obtained if one situates a square lattice instead of the nanodisk array. We have shown that the properties of the lattices in the vortex layer can be tuned to alter the skyrmion properties in the skyrmion layer. The lattice sizes are chosen according to well-established fabrication techniques, where one can use an electron beam or photon lithography to pattern the nanodisks and square lattice.

In this paper, the (anti)vortex and (anti)skyrmion cores are ferromagnetically coupled. Hence, it is possible to delete the (anti)skyrmions by applying a short IP magnetic field pulse or a charge current. Our numerical investigations indicate that the writing process using short field pulses is not as reliable as the OOP field nucleation method. We have demonstrated with our numerical experiments that the skyrmions can be deleted reliably by short pulses of IP magnetic fields or charge currents that lead to a STT in the vortex and skyrmion layer. Although the same principle holds for antiskyrmions, the annihilation process seems to be less correlated to the antivortex-core reversal. Note that we are using metallic multilayers as the skyrmionic host layer. Thus, the current is expected to flow in both layers simultaneously, as we have modeled in our simulations. However, one could even think of using garnets with perpendicular magnetic anisotropy, which are well-known ferrimagnetic insulators [44]. Doing so, one could avoid the STT acting directly on the skyrmions and ensure a better writing or deleting process.

In general, the main application of the proposed concept was to generate and annihilate (anti)skyrmions for a skyrmionic device such as magnetic racetrack memory [23], where skyrmions and antiskyrmions can be used to encode information. Furthermore, our findings might find application in reservoir computing. Since the skyrmions are coupled to the vortices above, a skyrmionic fabric with pinned skyrmions and thus, reproducible responses could be obtained [14,15] by designing the vortex layers.

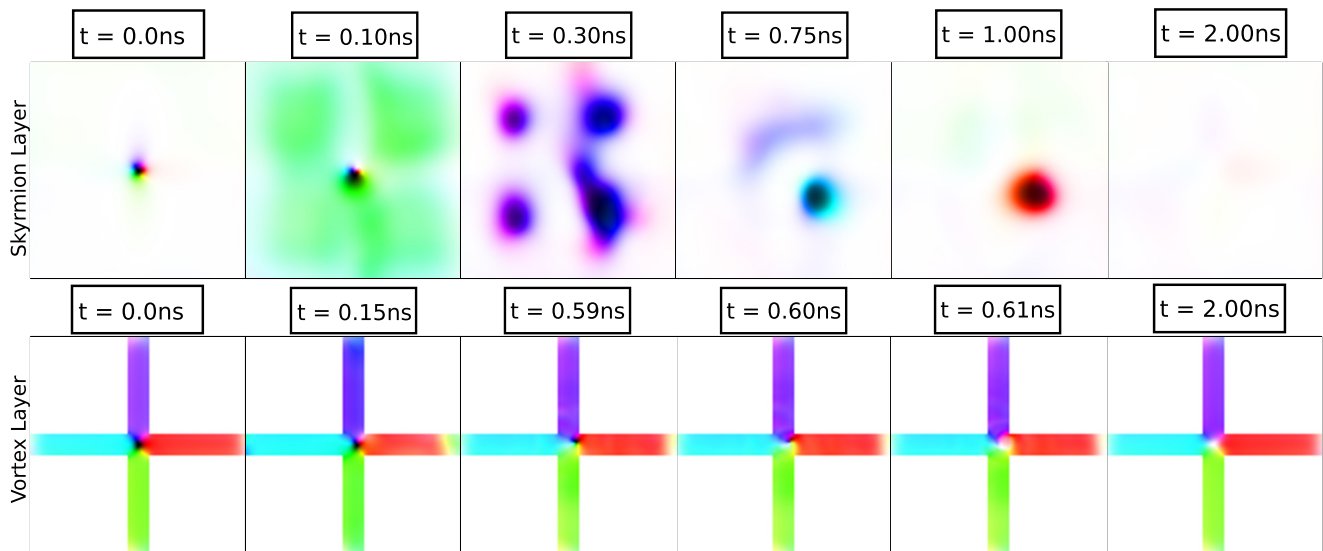


FIG. 10. Same as Fig. 6 but for the antiskyrmions deletion process in the SkL progresses via the antivortex core reversal in the VL above.

ACKNOWLEDGMENTS

The computational results presented have been achieved in part using the Vienna Scientific Cluster (VSC). F.B. and D.S. gratefully acknowledge the Austrian Science Fund (FWF) for support through Grant No. I 4917 (MagFunc). S.K. and C.A. gratefully acknowledge the Austrian Science Fund (FWF) for

support through Grant No. P34671 (Vladimir). S.K. and D.S. acknowledge the Austrian Science Fund (FWF) for support through Grant No. I 6267 (CHIRALSPIN). M.A. gratefully acknowledges funding from the Deutsche Forschungsgemeinschaft (DFG, German Research Foundation) Grant No. 507821284.

- [1] A. Bogdanov and A. Hubert, Thermodynamically stable magnetic vortex states in magnetic crystals, *J. Magn. Magn. Mater.* **138**, 255 (1994).
- [2] A. N. Bogdanov, U. K. Rößler, M. Wolf, and K.-H. Müller, Magnetic structures and reorientation transitions in noncentrosymmetric uniaxial antiferromagnets, *Phys. Rev. B* **66**, 214410 (2002).
- [3] S. Mühlbauer, B. Binz, F. Jonietz, C. Pfleiderer, A. Rosch, A. Neubauer, R. Georgii, and P. Böni, Skyrmion lattice in a chiral magnet, *Science* **323**, 915 (2009).
- [4] X. Z. Yu, Y. Onose, N. Kanazawa, J. H. Park, J. H. Han, Y. Matsui, N. Nagaosa, and Y. Tokura, Real-space observation of a two-dimensional skyrmion crystal, *Nature (London)* **465**, 901 (2010).
- [5] O. Boulle, J. Vogel, H. Yang, S. Pizzini, D. de Souza Chaves, A. Locatelli, T. O. Menteş, A. Sala, L. D. Buda-Prejbeanu, O. Klein, M. Belmeguenai, Y. Roussigné, A. Stashkevich, S. M. Chérif, L. Aballe, M. Foerster, M. Chshiev, S. Auffret, I. M. Miron, and G. Gaudin, Room-temperature chiral magnetic skyrmions in ultrathin magnetic nanostructures, *Nat. Nanotechnol.* **11**, 449 (2016).
- [6] K. Everschor-Sitte, J. Masell, R. M. Reeve, and M. Kläui, Perspective: Magnetic skyrmions—overview of recent progress in an active research field, *J. Appl. Phys.* **124**, 240901 (2018).
- [7] A.-O. Mandru, O. Yildirim, R. Tomasello, P. Heistracher, M. Penedo, A. Giordano, D. Suess, G. Finocchio, and H. J. Hug, Coexistence of distinct skyrmion phases observed in hybrid ferromagnetic/ferrimagnetic multilayers, *Nat. Commun.* **11**, 6365 (2020).
- [8] S. A. Montoya, S. Couture, J. J. Chess, J. C. T. Lee, N. Kent, D. Henze, S. K. Sinha, M.-Y. Im, S. D. Kevan, P. Fischer, B. J. McMorran, V. Lomakin, S. Roy, and E. E. Fullerton, Tailoring magnetic energies to form dipole skyrmions and skyrmion lattices, *Phys. Rev. B* **95**, 024415 (2017).
- [9] S. A. Montoya, S. Couture, J. J. Chess, J. C. T. Lee, N. Kent, M.-Y. Im, S. D. Kevan, P. Fischer, B. J. McMorran, S. Roy, V. Lomakin, and E. E. Fullerton, Resonant properties of dipole skyrmions in amorphous Fe/Gd multilayers, *Phys. Rev. B* **95**, 224405 (2017).
- [10] M. Heigl, S. Koraltan, M. Vaňatka, R. Kraft, C. Abert, C. Vogler, A. Semisalova, P. Che, A. Ullrich, T. Schmidt, J. Hintermayr, D. Grundler, M. Farle, M. Urbánek, D. Suess, and M. Albrecht, Dipolar-stabilized first and second-order antiskyrmions in ferrimagnetic multilayers, *Nat. Commun.* **12**, 2611 (2021).
- [11] G. Finocchio, F. Büttner, R. Tomasello, M. Carpentieri, and M. Kläui, Magnetic skyrmions: From fundamental to applications, *J. Phys. D: Appl. Phys.* **49**, 423001 (2016).
- [12] S. S. Parkin, M. Hayashi, and L. Thomas, Magnetic domain-wall racetrack memory, *Science* **320**, 190 (2008).
- [13] N. S. Kiselev, A. Bogdanov, R. Schäfer, and U. Rößler, Chiral skyrmions in thin magnetic films: New objects for magnetic storage technologies? *J. Phys. D: Appl. Phys.* **44**, 392001 (2011).
- [14] G. Bourianoff, D. Pinna, M. Sitte, and K. Everschor-Sitte, Potential implementation of reservoir computing models based on magnetic skyrmions, *AIP Adv.* **8**, 055602 (2018).
- [15] D. Prychynenko, M. Sitte, K. Litzius, B. Krüger, G. Bourianoff, M. Kläui, J. Sinova, and K. Everschor-Sitte, Magnetic

- skyrmion as a nonlinear resistive element: A potential building block for reservoir computing, *Phys. Rev. Appl.* **9**, 014034 (2018).
- [16] C. Back, V. Cros, H. Ebert, K. Everschor-Sitte, A. Fert, M. Garst, T. Ma, S. Mankovsky, T. L. Monchesky, M. Mostovoy, N. Nagaosa, S. S. P. Parkin, C. Pfleiderer, N. Reyren, A. Rosch, Y. Taguchi, Y. Tokura, K. von Bergmann, and J. Zang, The 2020 skyrmionics roadmap, *J. Phys. D* **53**, 363001 (2020).
- [17] X. Zhang, Y. Zhou, K. Mee Song, T.-E. Park, J. Xia, M. Ezawa, X. Liu, W. Zhao, G. Zhao, and S. Woo, Skyrmion-electronics: Writing, deleting, reading and processing magnetic skyrmions toward spintronic applications, *J. Phys.: Condens. Matter* **32**, 143001 (2020).
- [18] A. Fert, V. Cros, and J. Sampaio, Skyrmions on the track, *Nat. Nanotechnol.* **8**, 152 (2013).
- [19] D. Suess, C. Vogler, F. Bruckner, P. Heistracher, and C. Abert, A repulsive skyrmion chain as a guiding track for a racetrack memory, *AIP Adv.* **8**, 115301 (2018).
- [20] D. Suess, C. Vogler, F. Bruckner, P. Heistracher, F. Slanovc, and C. Abert, Spin torque efficiency and analytic error rate estimates of skyrmion racetrack memory, *Sci. Rep.* **9**, 4827 (2019).
- [21] A. K. Nayak, V. Kumar, T. Ma, P. Werner, E. Pippel, R. Sahoo, F. Damay, U. K. Röbber, C. Felser, and S. S. P. Parkin, Magnetic antiskyrmions above room temperature in tetragonal Heusler materials, *Nature (London)* **548**, 561 (2017).
- [22] J. Jena, R. Stinshoff, R. Saha, A. K. Srivastava, T. Ma, H. Deniz, P. Werner, C. Felser, and S. S. P. Parkin, Observation of magnetic antiskyrmions in the low magnetization ferrimagnet $\text{Mn}_2\text{Rh}_{0.95}\text{Ir}_{0.05}\text{Sn}$, *Nano Lett.* **20**, 59 (2020).
- [23] M. Hoffmann, G. P. Müller, C. Melcher, and S. Blügel, Skyrmion-antiskyrmion racetrack memory in rank-one dmi materials, *Front. Phys.* **9**, 769873 (2021).
- [24] J. Jena, B. Göbel, T. Ma, V. Kumar, R. Saha, I. Mertig, C. Felser, and S. S. P. Parkin, Elliptical Bloch skyrmion chiral twins in an antiskyrmion system, *Nat. Commun.* **11**, 1115 (2020).
- [25] L. Peng, R. Takagi, W. Koshibae, K. Shibata, K. Nakajima, T.-h. Arima, N. Nagaosa, S. Seki, X. Yu, and Y. Tokura, Controlled transformation of skyrmions and antiskyrmions in a non-centrosymmetric magnet, *Nat. Nanotechnol.* **15**, 181 (2020).
- [26] C. Felser and S. Parkin, Topology, skyrmions, and heusler compounds, *MRS Bull.* **47**, 600 (2022).
- [27] Y. Liu, S. Gliga, R. Hertel, and C. Schneider, Current-induced magnetic vortex core switching in a permalloy nanodisk, *Appl. Phys. Lett.* **91**, 112501 (2007).
- [28] F. Bruckner, S. Koraltan, C. Abert, and D. Suess, magnum.np: A PyTorch based GPU enhanced finite difference micromagnetic simulation framework for high level development and inverse design, *Sci. Rep.* **13**, 12054 (2023).
- [29] C. Abert, Micromagnetics and spintronics: Models and numerical methods, *Eur. Phys. J. B* **92**, 1 (2019).
- [30] M.-Y. Im, P. Fischer, K. Yamada, T. Sato, S. Kasai, Y. Nakatani, and T. Ono, Symmetry breaking in the formation of magnetic vortex states in a permalloy nanodisk, *Nat. Commun.* **3**, 983 (2012).
- [31] U. B. Arnalds, M. Ahlberg, M. S. Brewer, V. Kapaklis, E. T. Papaioannou, M. Karimipour, P. Korelis, A. Stein, S. Ólafsson, T. Hase *et al.*, Thermal transitions in nano-patterned xy-magnets, *Appl. Phys. Lett.* **105**, 042409 (2014).
- [32] K. Y. Guslienko, V. Novosad, Y. Otani, H. Shima, and K. Fukamichi, Magnetization reversal due to vortex nucleation, displacement, and annihilation in submicron ferromagnetic dot arrays, *Phys. Rev. B* **65**, 024414 (2001).
- [33] R. F. Wang, C. Nisoli, R. S. Freitas, J. Li, W. McConville, B. J. Cooley, M. S. Lund, N. Samarth, C. Leighton, V. H. Crespi, and P. Schiffer, Artificial 'spin ice' in a geometrically frustrated lattice of nanoscale ferromagnetic islands, *Nature (London)* **439**, 303 (2006).
- [34] S. H. Skjærø, C. H. Marrows, R. L. Stamps, and L. J. Heyderman, Advances in artificial spin ice, *Nat. Rev. Phys.* **2**, 13 (2020).
- [35] C. Nisoli, R. Moessner, and P. Schiffer, *Colloquium*: Artificial spin ice: Designing and imaging magnetic frustration, *Rev. Mod. Phys.* **85**, 1473 (2013).
- [36] S. Koraltan, M. Pancaldi, N. Leo, C. Abert, C. Vogler, K. Hofhuis, F. Slanovc, F. Bruckner, P. Heistracher, M. Menniti, P. Vavassori, and D. Suess, Dependence of energy barrier reduction on collective excitations in square artificial spin ice: A comprehensive comparison of simulation techniques, *Phys. Rev. B* **102**, 064410 (2020).
- [37] See Supplemental Material at <http://link.aps.org/supplemental/10.1103/PhysRevB.108.134401> for energy barrier calculations and more detailed simulations on tunability of the geometry, and current induced annihilation of skyrmions.
- [38] A. Farhan, P. M. Derlet, A. Kleibert, A. Balan, R. V. Chopdekar, M. Wyss, J. Perron, A. Scholl, F. Nolting, and L. J. Heyderman, Direct observation of thermal relaxation in artificial spin ice, *Phys. Rev. Lett.* **111**, 057204 (2013).
- [39] K. Hofhuis, A. Hrabec, H. Arava, N. Leo, Y.-L. Huang, R. V. Chopdekar, S. Parchenko, A. Kleibert, S. Koraltan, C. Abert, C. Vogler, D. Suess, P. M. Derlet, and L. J. Heyderman, Thermally superactive artificial kagome spin ice structures obtained with the interfacial Dzyaloshinskii-Moriya interaction, *Phys. Rev. B* **102**, 180405 (2020).
- [40] R. Hertel, S. Gliga, M. Fähnle, and C. M. Schneider, Ultrafast nanomagnetic toggle switching of vortex cores, *Phys. Rev. Lett.* **98**, 117201 (2007).
- [41] S. Gliga, R. Hertel, and C. M. Schneider, Switching a magnetic antivortex core with ultrashort field pulses, *J. Appl. Phys.* **103**, 07B115 (2008).
- [42] S. Gliga, Y. Liu, and R. Hertel, Energy thresholds in the magnetic vortex core reversal, *J. Phys.: Conf. Ser.* **303**, 012005 (2011).
- [43] B. Van Waeyenberge, A. Puzic, H. Stoll, K. W. Chou, T. Tylliszczak, R. Hertel, M. Fähnle, H. Brückl, K. Rott, G. Reiss, I. Neudecker, D. Weiss, C. H. Back, and G. Schütz, Magnetic vortex core reversal by excitation with short bursts of an alternating field, *Nature (London)* **444**, 461 (2006).
- [44] C. Holzmann, A. Ullrich, O.-T. Ciubotariu, and M. Albrecht, Stress-induced magnetic properties of gadolinium iron garnet nanoscale-thin films: Implications for spintronic devices, *ACS Appl. Nano Mater.* **5**, 1023 (2022).